Article

Nonlinear Optical Crystal Rb4Sn3Cl2Br8: Synthesis, Structure, and Characterization

Pifu Gong, Siyang Luo, Yi Yang, Fei Liang, Shengzi Zhang, Sangen Zhao, Junhua Luo, and Zheshuai Lin

Cryst. Growth Des., **Just Accepted Manuscript** • DOI: 10.1021/acs.cgd.7b01373 • Publication Date (Web): 20 Nov 2017

Nonlinear Optical Crystal $Rb_4Sn_3Cl_2Br_8$: Synthesis, Structure, and Characterization

Pifu Gong,[†] Siyang Luo,[†] Yi Yang,[†,‡] Fei Liang,[†,‡] Shengzi Zhang,[†,‡] Sangen Zhao,[§] Junhua Luo,[§] and Zheshuai Lin[†,‡,*]

[†]Technical Institute of Physics and Chemistry, Chinese Academy of Sciences, Beijing 100190, China.

[‡] University of the Chinese Academy of Sciences, Beijing 100049, China.

[§] State Key Laboratory of Structural Chemistry, Institute of Research on the Structure of Matter, Chinese Academy of Sciences, Fuzhou, Fujian 350002, China

ABSTRACT: A new Sn-based halide compound, $Rb_4Sn_3Cl_2Br_8$, is synthesized by hydrothermal method. This compound crystallizes in orthorhombic noncentrosymmetric space group of $Cmc2_1$, and the structure is composed of one-dimensional $[Sn_4Cl_2Br_8]^1_\infty$ chains elongated in parallel to *a*-axis. Interestingly, in the $[Sn_4Cl_2Br_8]^1_\infty$ chains the $[SnBr_5]$ and $[SnClBr_4]$ groups hold pyramidal configurations which are found for the first time in Sn-based metal halides. $Rb_4Sn_3Cl_2Br_8$ exhibits a high thermal stability (up to 270 °C) and a relatively large bandgap of 2.82 eV. This compound shows a phase-matchable powder second harmonic generation response of 0.5 times of KH_2PO_4 (KDP), and is the first phase-matchable Sn-based halide nonlinear optical material. The discovery of $Rb_4Sn_3Cl_2Br_8$ will be beneficial to further phase-matchable nonlinear optical materials exploration in Sn-based halides.

1. Introduction

Recently, metal halides compounds have been intensively studied for their special structural features and excellent photoelectric properties.[1-8] Typically, the fundamental building units in metal halides are $[MX_k]$, where *M* is the central metal cation and *X* is the halide anion with *k* varying from 2 to 6.[9-13] Their various connecting modes led to the pronounced structural diversity and the resulted metal halides serving as a new class of photoelectric materials widely used in photovoltaics, light emitting diodes (LEDs), nonlinear optical (NLO) materials, lasers, and photodetectors.[14-19] For example, $Cs_2HgI_2Cl_2$, $Rb_2CdBr_2I_2$, and $K_2SbF_2Cl_3$ can be used as infrared NLO materials, which have been considered to achieve the balance between the NLO responses and laser damage thresholds.[20-25] The organic-inorganic hybrid halides perovskites, especially $CH_3NH_3PbI_3$, using as the light absorbing materials in solar cells, have successfully improved the power conversion efficiency to ~ 22.1%.[15, 26] For the remarkable optical and electric properties, it is of great interest in pursuing new metal halide compounds.

Attributed to the environmentally friendly feature, new tin(II)-based halides have increased explosively in the lead-free perovskite solar cells since the first report involving $CH_3NH_3SnI_3$ in 2014.[27-30] Moreover, the presence of stereoactive lone-pair electrons (LPE) on Sn can lead to many fantastic photoelectric features, including photocatalysis and NLO properties.[31-34] It is well known that the ordered LPE arrangement can produce a large NLO response, and, thus, the Sn-based halides possess great potential to be promising NLO materials.[35,36] However, till now, only two Sn-based halides, $NH(CH_3)_3SnCl_3$ and $NH(CH_3)_3SnBr_3$,[37] have been reported to exhibit NLO effect, and the absence of phase-matching capability limits their practical applications.

To enrich the structural diversity and photoelectric functions, our group has been carrying out material explorations and performance characterizations in the Sn-based halides compounds.[32, 38] In this work, we successfully synthesize the first phase-matching Sn-based halide NLO material $Rb_4Sn_3Cl_2Br_8$. This compound exhibits a high thermal stability (up to 270 °C) and a relatively large bandgap of 2.82 eV with the phase-matchable powder second harmonic generation (SHG) response of 0.5 times of KH_2PO_4 (KDP).

2. Experimental Section

2.1. Single Crystal Growth

Single crystals of $Rb_4Sn_3Cl_2Br_8$ were grown by hydrothermal method using RbCl (Aladdin, 99.0%), $SnCl_2•2H_2O$ (SCR, 98.0%) and HBr (Aladdin, 40%) as the raw materials. About 1g (0.0238 mol) RbCl, 1g (0.0044 mol) $SnCl_2•2H_2O$, and 1ml HBr were dissolved in H_2O (3.0 mL). The fully mixed solution was sealed in an autoclave equipped with a Teflon liner (25 ml) and heated at 220 °C for 1 day and further slowly cooled to the room temperature at a rate of 3 °C/h. The reacting product was washed with ethanol and dried in air. The colorless transparent crystals of Rb_2SnCl_6 and light green transparent crystals of $Rb_4Sn_3Cl_2Br_8$ with millimeter size were obtained.

2.2. Single-Crystal Structure Determination

The single crystal X-ray diffraction (XRD) measurements were performed on a Rigaku AFC10 diffractometer (Mo Kα, λ = 0.71073 Å radiation) equipped with a graphite monochromator. The Crystalclear software[39]

was used for data extraction and integration and the program XPREP was used for face-indexed absorption corrections. The structures were solved by direct methods using SHELXS-97 and then refined by full-matrix least-squares refinement on F^2 with SHELXL-97 found in the software suite WinGX.[40, 41] The structures were verified using the ADDSYM algorithm from the program PLATON,[42] and no higher symmetries were found.

2.3. Powder X-ray Diffraction

The powder X-ray diffraction (PXRD) pattern of the polycrystalline $Rb_4Sn_3Cl_2Br_8$ was performed at room temperature using an automated Bruker D8 Focus X-ray diffractometer equipped with a diffracted monochromator set for Cu Kα (λ = 1.5418 Å) radiation. The scanning step width of 0.02° and the scanning rate of 0.1° s^{-1} were applied to record the patterns in the 2 theta range of 10-70°. The experimental powder X-ray diffraction pattern was found to be in good agreement with the theoretical pattern calculated on the based of single crystal crystallographic data (Figure S1).

2.4. UV-Vis-NIR Diffuse Reflectance Spectroscopy

UV–vis–NIR diffuse reflectance data for $Rb_4Sn_3Cl_2Br_8$ were collected with a SolidSpec-3700 DUV spectrophotometer in the wavelength range from 200 to 1400 nm. Fluororesin was applied as the standard.

2.5. Thermal Stability Measurement

About 10 mg of $Rb_4Sn_3Cl_2Br_8$ were used for the thermogravimetric (TG) analysis measurement by the NETZSCH STA-409CD thermal analyzer. The sample was placed in platinum crucible and heated from room temperature to 850°C at the rate of 20 °C/min. The melted residue were examined and analyzed by PXRD.

2.6 Nonlinear Optical Property

Powder SHG measurements were carried out by the Kuttz-Perry method.[43] A pulsed Q-switched Nd:YAG laser was utilized to generate fundamental 1064 nm light with a pulse width of 5 ns. As powder SHG effect depends strongly on the particle size, $Rb_4Sn_3Cl_2Br_8$ crystals were ground and sieved into the following particle size ranges: 48-75，75-106，106-125，125-180, 180-230, and 230-250 um, respectively. KDP was also ground and sieved into the same particle size ranges and used as references for SHG measurements.

2.7. Computational Method

The first-principles calculations were performed using the plane-wave pseudopotential method implemented in the CASTEP package.[44] The generalized gradient approximation (GGA)[45] with the Perdew, Burke and Ernzerhof (PBE) functionals[46] and the optimized norm-conserving pseudopotentials in the Kleinman-Bylander form[47] are adopted in the calculations. Rb $4s^24p^65p^1$, Sn $5s^25p^2$, Cl $3s^23p^5$, and Br $4s^24p^5$ are treated as valence electrons. The kinetic energy cutoff of 900 eV and Monkhorst–Pack 2×2×2 k-point meshes[48] are used. The choice of these computational parameters is good enough to ensure the accuracy of present purpose.

3. Results and Discussion

3.1. Single crystal growth

Single crystals of $Rb_4Sn_3Cl_2Br_8$ were obtained by the hydrothermal method in a yield of about 57% based on Sn with the raw materials and reaction conditions described in the experimental section. The chemical reaction is proposed as:

$$4RbCl + 3SnCl_2 + 8HBr \rightarrow Rb_4Sn_3Cl_2Br_8 \downarrow + 8HCl$$

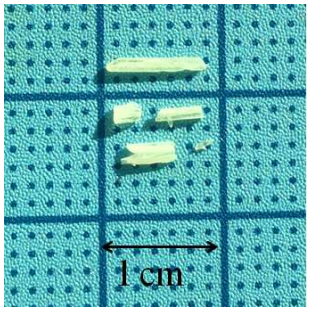

Figure 1. The photograph of $Rb_4Sn_3Cl_2Br_8$ crystal

After the reaction, the light green transparent crystals with millimeter size were obtained and their photograph is shown in Figure 1. The crystal structure was solved and refined on the basis of single crystal XRD data. The PXRD pattern (Figure S1b) of the obtained crystals show good agreement with the calculated results (Figure S1a) derived from the single crystal data (Table 1, Table S1-3).

Table 1. Crystal data and structure refinement for $Rb_4Sn_3Cl_2Br_8$

	$Rb_4Sn_3Cl_2Br_8$
Formula weight	1407.83
Crystal system	Orthorhombic
Space group	$Cmc2_1$
Unit cell dimensions	a = 10.0279(6) Å b = 17.7490(12) Å c = 12.5827(7) Å
Volume	2239.5(2) $Å^3$
Z	4
Density	4.175 mg/m^3
Absorption coefficient	26.449 mm^{-1}
GOF on F^2	1.127
Final R [$F_o^2 > 2\sigma(F_o^2)$]	R_1 = 0.0535, wR_2 = 0.1610
R (all data)	R_1 = 0.0578, wR_2 = 0.1641

3.2. Crystal structure

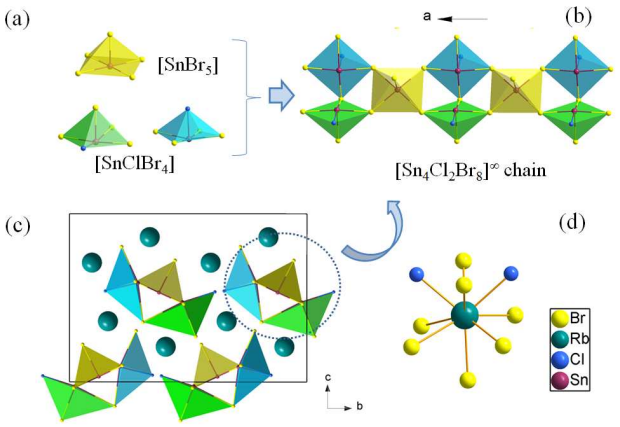

Figure 2. (a) The $[SnBr_5]$ and $[SnClBr_4]$ groups, (b) the $[Sn_4Cl_2Br_8]^1_\infty$ chain, (c) the crystal structure of $Rb_4Sn_3Cl_2Br_8$, and (d) the coordinating environment of Rb cation.

The structure of $Rb_4Sn_3Cl_2Br_8$ is illustrated in Figure 2. This compound crystallizes in the orthorhombic space group of *Cmc*2$_1$ (No. 36) with unit cell parameters a = 10.0279(6) Å, b = 17.7490(12) Å, c = 12.5827(7) Å. In the symmetric unit, Rb, Sn, Cl, and Br occupy two, three, two, and six crystallographically unique positions, respectively, with all the atoms located at Wyckoff positions of *4a*. All Sn atoms are five-fold coordinated with halogen atoms to form either $[SnBr_5]$ (yellow color in Figure 2a) or $[SnClBr_4]$ pyramids ($[Sn1ClBr_4]$ in green color and $[Sn2ClBr_4]$ in blue color, respectively, in Figure 2a). The $[Sn1ClBr_4]$ and $[Sn2ClBr_4]$ units can be considered as the derivatives of $[SnBr_5]$ units with the corner and apex Br atoms replaced by Cl atoms, respectively. These $[SnBr_5]$ and $[SnClBr_4]$ pyramids connect with one another by sharing the Br atoms and construct $[Sn_4Cl_2Br_8]^1_\infty$ chains along the *a*-axis (see Figure 2b). The strong anisotropy resulted from the chained structure is reflected in the morphology of the obtained crystals which are displayed in Figure 1. The $[Sn_4Cl_2Br_8]^1_\infty$ chains are parallel in the *a*-*b* plane, while in the neighboring plane the chains are anti-parallel arranged and rotated about 55° (see Figure 2c), which would result in certain NLO effects in $Rb_4Sn_3Cl_2Br_8$. The Rb^+ cations are located in the interstices among the chains and each Rb^+ coordinates with seven F^- and two Cl^- anions (see Figure 2d).

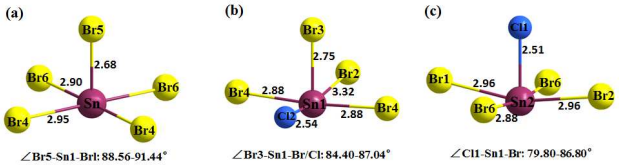

Figure 3. The local coordinating environments of Sn atoms in $Rb_4Sn_3Cl_2Br_8$.

The local coordinating environments of Sn atoms in $Rb_4Sn_3Cl_2Br_8$ are shown in Figure 3. Interestingly, the $[SnX_5]$ groups are very rarely found in the Sn-based metal halides compounds in which only three types of $[SnX_5]$ groups have been reported, *i.e.*, $[SnF_5]$, $[SnCl_5]$, and $[SnF_3Cl_2]$, and all of them possess the pseudo-octohedral configurations, according to our survey in the Inorganic Crystal Structure Database (ICSD).[49] The $[SnBr_5]$ and $[SnClBr_4]$ groups presented in $Rb_4Sn_3Cl_2Br_8$ are found for the first time. Moreover, it is unique that both these fundamental building blocks manifest the pyramidal shapes with the Sn atoms almost located in the base surface. In $[SnBr_5]$, the dangling Sn-Br bond is about 2.7 Å and the bridging ones are about 2.9 Å with the vertical Br-Sn-Br angles about 90°, which makes this group almost hold the standard pyramidal configuration (Figure 3a). The introduction of Cl^- anions in the $[SnClBr_4]$ pyramids results in the great distortion compared with the $[SnBr_5]$ pyramids since the Sn-Br/Cl bonds vary from 2.51 to 3.32 Å and the vertical Br-Sn-Br/Cl angles vary from 79.80 to 87.04° (Figure 3b and 3c). The first-principles charge density difference around the $[SnBr_5]$ and $[SnClBr_4]$ units is exhibited in Figure 4. Clearly, the LPE on Sn^{2+} cations hinder the formation of chemical bonds to the neighboring Br atoms from the same side. Meanwhile, the corner Br atoms effectively push one another to the opposite orientation in the $[SnBr_5]$ pyramidal unit, which produces enough space to accommodate Sn^{2+} cations located in the base surface. When the corner or the apex Br atoms are replaced by smaller Cl atoms in the $[SnClBr_4]$ units, the Sn^{2+} cations are slightly squeezed out of the base surface, leading to the distorted pyramidal configurations. The discovery of $[SnBr_5]$ and $[SnClBr_4]$ pyramidal units definitely enriches the structural diversity in metal halides.

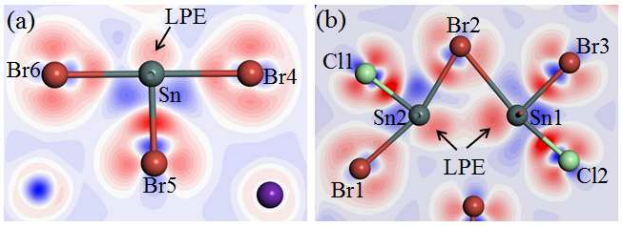

Figure 4. Charge density difference around (a) $[SnBr_5]$ and (b) $[Sn1ClBr_4]$ and $[Sn2ClBr_4]$ units

3.3. Thermal properties

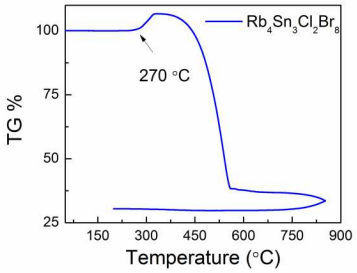

Figure 5. The TG curve of $Rb_4Sn_3Cl_2Br_8$.

The thermal measurement for the titled compound is shown in Figure 5. The TG analysis curves exhibit that the weight firstly increases and then decreases with the total weight losses about 70%. The weight change starts at 270 °C, indicating that $Rb_4Sn_3Cl_2Br_8$ is stable under this temperature. The PXRD patterns of the title compound before and after heating (shown in Figure S1) reveal that the melted residue is SnO_2 after heating above 270 °C, which means that the decomposition reaction can attributed to:

$$Rb_4Sn_3Cl_2Br_8 + 3O_2 \rightarrow 3SnO_2 + 4RbBr\uparrow + Cl_2\uparrow$$

From the chemical equation, one may easily obtain that the theoretical mass residues is about 32.2% for $Rb_4Sn_3Cl_2Br_8$, in good agreement with the experimental results.

3.4. Optical properties

The UV-vis-NIR diffuse-reflectance spectrum for $Rb_4Sn_3Cl_2Br_8$ is shown in Figure 6. It is revealed that the optical absorption edge of the title compound is about 440 nm, corresponding to the energy bandgap of 2.82 eV. The relatively large band gap also indicates the relatively high laser damage threshold that is valuable for practical applications.[50-52]

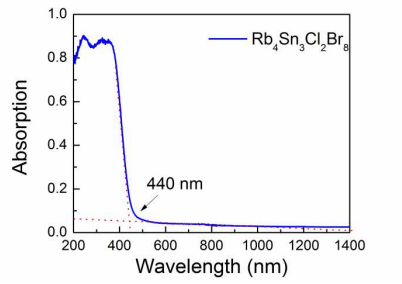

Figure 6. The UV-vis-NIR diffuse-reflectance spectrum of $Rb_4Sn_3Cl_2Br_8$.

Owing to the noncentrosymmestic space group, $Rb_4Sn_3Cl_2Br_8$ would exhibit the second order NLO response. The powder SHG measurements using 1064 nm radiation revealed that the SHG effect of $Rb_4Sn_3Cl_2Br_8$ is about 0.5 times as strong as that of KDP. Moreover, as shown in Figure 7, the SHG intensities grows gradually as the particle size increases until it reaches a plateau above 200 μm, which indicates that $Rb_4Sn_3Cl_2Br_8$ is a phase-matchable crystal and it is the first compound found in the Sn-based halides nonlinear optical materials.

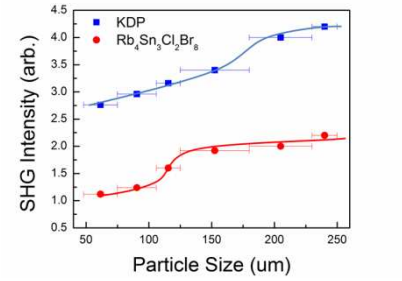

Figure 7. Dependence of SHG intensity on the particle size for $Rb_4Sn_3Cl_2Br_8$.

3.5. First-principles calculations

The electronic structure in $Rb_4Sn_3Cl_2Br_8$ is investigated by the first-principles calculations using the CASTEP package. As shown in Figure 8a, both the valence band (VB) maximum and the conduction band (CB) minimum are located at the G1 point indicating the direct bandgap characteristic. The calculated bandgap of 1.98 eV is slightly smaller than the experimental value of 2.82 eV, which is caused by the discontinuity of exchange-correlation energy implemented in the local density approximation (LDA).[53] Figure 8b shows the partial density of states (PDOS) nearby the bandgap projected on the constituent elements in $Rb_4Sn_3Cl_2Br_8$. It is clear that the top of the VB are composed of not only the *p*- orbitals of Cl^- (*3p*) and Br^- (*4p*) anions but also the *5s*- and *5p*- orbitals of Sn^{2+} cations. Meanwhile, the hybridization of Sn *5s5p* and Br *4p* orbitals dominantly contributes to the bottom of the CB. Therefore, the electronic states on both sides of the bandgap are mainly contributed by the $[SnBr_5]$ and $[SnClBr_4]$ groups, which determine optical properties of $Rb_4Sn_3Cl_2Br_8$, in consistence with the conclusion from anionic group theory proposed by Chen.[54]

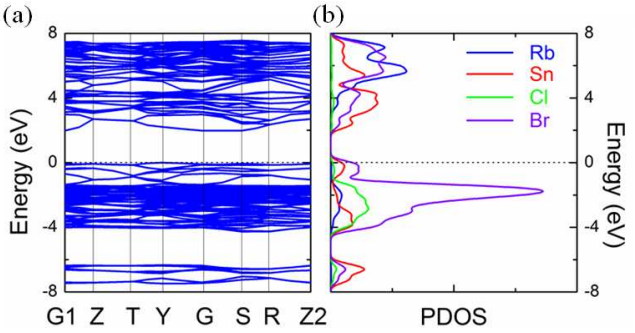

Figure 8. (a) The electronic band structure, and (b) PDOS plot of $Rb_4Sn_3Cl_2Br_8$.

The first-principles linear and nonlinear optical properties in $Rb_4Sn_3Cl_2Br_8$ are listed in Table2. The calculated powder SHG effect (~ 0.8×KDP) is in good agreement with the experimental results (~ 0.5×KDP), which verifies the validity of the pseudopotential method employed. Moreover, the relatively large birefringence (Δn > 0.2) at both the wavelength λ = 1064 nm and 2090 nm in $Rb_4Sn_3Cl_2Br_8$ indicates that this compound is easy to reach the phase-matching condition in the IR spectral region. From the point view of structure-property relationship, the large optical anisotropy is originated from the parallel arranged 1D $[Sn_4Cl_2Br_8]^1_\infty$ chains along the *a*-axis. However, the LPE on different Sn^{2+} cations in the chains point to different orientations, which attenuates the macro polarity, as shown in Figure S2, and thus leads to the relatively weak NLO effect in crystal.

Table 2. The calculated linear and nonlinear optical properties in $Rb_4Sn_3Cl_2Br_8$.

Refractive indices and birefringence			NLO coefficients (pm/V)	
λ (nm)	1064	2090		
n_x	2.2621	2.2114	d_{15}	0.28
n_y	2.0322	2.0045	d_{24}	0.28
n_z	2.0537	2.0241	d_{33}	-0.52
Δn	0.2299	0.2069	Powder SHG	0.31 (~0.8×KDP)

4. Conclusions

The first phase-matched Sn-based halide nonlinear optical crystal, $Rb_4Sn_3Cl_2Br_8$, is synthesized by hydrothermal method. This compound processes a one-dimensional (1D) structure consisted of the fundamental building units $[SnBr_5]$ and $[SnClBr_4]$ which hold the pyramid configuration and are found for the first time in the Sn-based metal halides. $Rb_4Sn_3Cl_2Br_8$ exhibits high

thermal stability (up to 270 °C) and a relatively large bandgap of 2.82 eV. Moreover, $Rb_4Sn_3Cl_2Br_8$ shows a phase-matchable powder SHG response of 0.5 times of KDP. The discovery of $Rb_4Sn_3Cl_2Br_8$ would provide a representative example of the research between structure and properties and it is beneficial for further exploration of nonlinear optical materials among the Sn-based halides.

ASSOCIATED CONTENT

Supporting Information.
The Supporting Information is available free of charge on the ACS Publications website at http://pubs.acs.org. CIF files and additional data.
Deposition CCDC number 1575046 for $Rb_4Sn_3Cl_2Br_8$.

AUTHOR INFORMATION

Corresponding Author

* zslin@mail.ipc.ac.cn.

Author Contributions.

All authors have given approval to the final version of the manuscript

Notes

The authors declare no competing financial interests.

ACKNOWLEDGMENT

This work was supported by "863" projects (Grant 2015AA034203) and NSF of China (Grants 91622118, 91622124, 11474292 and 51602318), and ZSL acknowledges the support from Youth Innovation Promotion Association, CAS.

REFERENCES

(1) Stoumpos, C. C.; Malliakas, C. D.; Kanatzidis, M. G. Semiconducting Tin and Lead Iodide Perovskites with Organic Cations: Phase Transitions, High Mobilities, and Near-Infrared Photoluminescent Properties. *Inorg. Chem.* **2013,** 52 (15), 9019-9038.
(2) Burschka, J.; Pellet, N.; Moon, S. J.; Humphry-Baker, R.; Gao, P.; Nazeeruddin, M. K.; Gratzel, M. Sequential deposition as a route to high-performance perovskite-sensitized solar cells. *Nature* **2013,** 499 (7458), 316.
(3) Dong, Q.; Fang, Y.; Shao, Y.; Mulligan, P.; Qiu, J.; Cao, L.; Huang, J. Electron-hole diffusion lengths > 175 mu m in solution-grown $CH_3NH_3PbI_3$ single crystals. *Science* **2015,** 347 (6225), 967-970.
(4) Xing, G.; Mathews, N.; Lim, S. S.; Yantara, N.; Liu, X.; Sabba, D.; Gratzel, M.; Mhaisalkar, S.; Sum, T. C. Low-temperature solution-processed wavelength-tunable perovskites for lasing. *Nat. Mater.* **2014,** 13 (5), 476-480.
(5) Wei, H.; Fang, Y.; Mulligan, P.; Chuirazzi, W.; Fang, H.-H.; Wang, C.; Ecker, B. R.; Gao, Y.; Loi, M. A.; Cao, L.; Huang, J. Sensitive X-ray detectors made of methylammonium lead tribromide perovskite single crystals. *Nat. Photonics* **2016,** 10 (5), 333.
(6) Atuchin, V. V.; Isaenko, L. I.; Kesler, V. G.; Tarasova, A. Y. Single crystal growth and surface chemical stability of KPb_2Br_5. *J. Cryst. Growth* **2011,** 318 (1), 1000-1004.
(7) Atuchin, V. V.; Isaenko, L. I.; Kesler, V. G.; Pokrovsky, L. D.; Tarasova, A. Y. Electronic parameters and top surface chemical stability of $RbPb_2Br_5$. *Mater. Chem. Phys.* **2012,** 132 (1), 82-86.
(8) Isaenko, L. I.; Goloshumova, A. A.; Yelisseyev, A. P.; Shubin, Y. V.; Khyzhun, O. Y.; Naumov, D. Y.; Tarasova, A. Y. New $SrPb_3Br_8$ crystals: Growth, crystal structure and optical properties. *J. Alloys Compd.* **2016,** 682, 832-838.
(9) Liu, T.; Qin, J.; Zhang, G.; Zhu, T.; Niu, F.; Wu, Y.; Chen, C. Mercury Bromide ($HgBr_2$): A promising nonlinear optical material in IR region with a high laser damage threshold. *Appl. Phys. Lett.* **2008,** 93 (9), 091102.
(10) Zhang, G.; Liu, T.; Zhu, T.; Qin, J.; Wu, Y.; Chen, C. SbF_3: A new second-order nonlinear optical material. *Opt. Mater.* **2008,** 31 (1), 110-113.
(11) Choi, M. H.; Kim, S. H.; Chang, H. Y.; Halasyamani, P. S.; Ok, K. M. New Noncentrosymmetric Material - $N(CH_3)_4ZnCl_3$: Polar Chains of Aligned $ZnCl_4$ Tetrahedra. *Inorg. Chem.* **2009,** 48 (17), 8376-8382.
(12) Tong, Y. Z.; Meng, X. Y.; Wang, Z. Z.; Chen, C. T.; Lee, M. H. The mechanism of linear and nonlinear optical effects in fluoride crystals. *J. Appl. Phys.* **2005,** 98 (3), 033504.
(13) Ren, P.; Qin, J. G.; Chen, C. T. A novel nonlinear optical crystal for the IR region: Noncentrosymmetrically crystalline CsCdBr3 and its properties. *Inorg. Chem.* **2003,** 42 (1), 8-10.
(14) Thirumal, K.; Chong, W. K.; Xie, W.; Ganguly, R.; Muduli, S. K.; Sherburne, M.; Asta, M.; Mhaisalkar, S.; Sum, T. C.; Soo, H. S.; Mathews, N. Morphology-Independent Stable White-Light Emission from Self-Assembled Two-Dimensional Perovskites Driven by Strong Exciton–Phonon Coupling to the Organic Framework. *Chem. Mater.* **2017,** 29 (9), 3947-3953.
(15) Xing, G.; Mathews, N.; Sun, S.; Lim, S. S.; Lam, Y. M.; Graetzel, M.; Mhaisalkar, S.; Sum, T. C. Long-Range Balanced Electron- and Hole-Transport Lengths in Organic-Inorganic $CH_3NH_3PbI_3$. *Science* **2013,** 342 (6156), 344-347.
(16) Zhu, H.; Fu, Y.; Meng, F.; Wu, X.; Gong, Z.; Ding, Q.; Gustafsson, M. V.; Trinh, M. T.; Jin, S.; Zhu, X. Y. Lead halide perovskite nanowire lasers with low lasing thresholds and high quality factors. *Nat. Mater.* **2015,** 14 (6), 636-U115.
(17) Weidman, M. C.; Goodman, A. J.; Tisdale, W. A. Colloidal Halide Perovskite Nanoplatelets: An Exciting New Class of Semiconductor Nanomaterials. *Chem. Mater.* **2017,** 29 (12), 5019-503.
(18) Zheng, X.; Liu, Y.; Liu, G.; Liu, J.; Ye, X.; Han, Q.; Ge, C.; Tao, X. Crystalline Mixed Halide Halobismuthates and Their Induced Second Harmonic Generation. *Chem. Mater.* **2016,** 28 (12), 4421-4431.
(19) Cho, H.; Jeong, S.-H.; Park, M.-H.; Kim, Y.-H.; Wolf, C.; Lee, C.-L.; Heo, J. H.; Sadhanala, A.; Myoung, N.; Yoo, S.; Im, S. H.; Friend, R. H.; Lee, T.-W. Overcoming the electroluminescence efficiency limitations of perovskite light-emitting diodes. *Science* **2015,** 350 (6265), 1222-1225.
(20) Wu, Q.; Meng, X.; Zhong, C.; Chen, X.; Qin, J. $Rb_2CdBr_2I_2$: A New IR Nonlinear Optical Material with a Large Laser Damage Threshold. *J. Am. Chem. Soc.* **2014,** 136 (15), 5683-5686.
(21) Zhang, G.; Li, Y.; Jiang, K.; Zeng, H.; Liu, T.; Chen, X.; Qin, J.; Lin, Z.; Fu, P.; Wu, Y.; Chen, C. A New Mixed Halide, $Cs_2HgI_2Cl_2$: Molecular Engineering for a New Nonlinear Optical Material in the Infrared Region. *J. Am. Chem. Soc.* **2012,** 134 (36), 14818-14822.
(22) Huang, Y.; Meng, X.; Gong, P.; Lin, Z.; Chen, X.; Qin, J. A study on $K_2SbF_2Cl_3$ as a new mid-IR nonlinear optical material: new synthesis and excellent properties. *J. Mater. Chem. C* **2015,** 3 (37), 9588-9593. 4.
(23) Bekenev, V. L.; Khyzhun, O. Y.; Sinelnichenko, A. K.; Atuchin, V. V.; Parasyuk, O. V.; Yurchenko, O. M.; Bezsmolnyy, Y.; Kityk, A. V.; Szkutnik, J.; Calus, S. Crystal growth and the electronic structure of Tl_3PbCl_5. *J. Phys. Chem. Solids* **2011,** 72 (6), 705-713.
(24) Atuchin, V. V.; Goloshumova, A. A.; Isaenko, L. I.; Jiang, X.; Lobanov, S. I.; Zhang, Z.; Lin, Z. Crystal growth and electronic structure of low-temperature phase $SrMgF_4$. *J. Solid State Chem.* **2016,** 236, 89-93.
(25) Parasyuk, O. V.; Khyzhun, O. Y.; Piasecki, M.; Kityk, I. V.; Lakshminarayana, G.; Luzhnyi, I.; Fochuk, P. M.; Fedorchuk, A. O.; Levkovets, S. I.; Yurchenko, O. M.; Piskach, L. V. Synthesis, structural, X-ray photoelectron spectroscopy (XPS) studies and IR induced anisotropy of Tl_4HgI_6 single crystals. *Mater. Chem. Phys.* **2017,** 187, 156-163.

(26) Saliba, M.; Matsui, T.; Seo, J.-Y.; Domanski, K.; Correa-Baena, J.-P.; Nazeeruddin, M. K.; Zakeeruddin, S. M.; Tress, W.; Abate, A.; Hagfeldt, A.; Gratzel, M. Cesium-containing triple cation perovskite solar cells: improved stability, reproducibility and high efficiency. *Energ. Environ. Sci.* **2016,** 9 (6), 1989-1997.
(27) Hao, F.; Stoumpos, C. C.; Cao, D. H.; Chang, R. P. H.; Kanatzidis, M. G. Lead-free solid-state organic-inorganic halide perovskite solar cells. *Nat. Photonics* **2014,** 8 (6), 489-494.
(28) Noel, N. K.; Stranks, S. D.; Abate, A.; Wehrenfennig, C.; Guarnera, S.; Haghighirad, A.-A.; Sadhanala, A.; Eperon, G. E.; Pathak, S. K.; Johnston, M. B.; Petrozza, A.; Herz, L. M.; Snaith, H. J. Lead-free organic-inorganic tin halide perovskites for photovoltaic applications. *Energ. Environ. Sci.* **2014,** 7 (9), 3061-3068.
(29) Zhang, C.; Gao, L.; Hayase, S.; Ma, T. Current Advancements in Material Research and Techniques Focusing on Lead-free Perovskite Solar Cells. *Chem. Lett.* **2017,** 46 (9), 1276-1284.
(30) Dimesso, L.; Fasel, C.; Lakus-Wollny, K.; Mayer, T.; Jaegermann, W. Thermal stability of lead-free $CH_3NH_3Sn_xI_3$ systems ($0.9 \leq x \leq 1.1$) for photovoltaics. *Mater. Sci. Semicond. Process.* **2017,** 68, 152-158.
(31) Pearson, R. G. A symmetry rule for predicting molecular strucre and reactivity *J. Am. Chem. Soc.* **1969,** 91 (5), 1252.
(32) Gong, P.; Luo, S.; Xiao, K.; Huang, Q.; Yang, Y.; Huang, H.; Wu, Y.; Chen, C.; Lin, Z. Structure and Characterization of a Zero-Dimensional Alkali Tin Dihalides Compound $Cs_3Sn_3F_2CI_7$ with the $Sn_2F_2CI_4^{2-}$ Clusters. *Inorg. Chem.* **2017,** 56 (5), 3081-3086.
(33) Chung, I.; Song, J. H.; Im, J.; Androulakis, J.; Malliakas, C. D.; Li, H.; Freeman, A. J.; Kenney, J. T.; Kanatzidis, M. G. $CsSnI_3$: Semiconductor or Metal? High Electrical Conductivity and Strong Near-Infrared Photoluminescence from a Single Material. High Hole Mobility and Phase-Transitions. *J. Am. Chem. Soc.* **2012,** 134 (20), 8579-8587.
(34) Lin, H.; Chen, L.; Yu, J.-S.; Chen, H.; Wu, L.-M. Infrared SHG Materials CsM_3Se_6 (M = Ga/Sn, In/Sn): Phase Matchability Controlled by Dipole Moment of the Asymmetric Building Unit. *Chem. Mater.* **2017,** 29 (2), 499-503.
(35) Hellwig, H.; Liebertz, J.; Bohaty, L. Exceptional large nonlinear optical coefficients in the monoclinic bismuth borate BiB_3O_6 (BIBO). *Solid State Commun.* **1999,** 109 (4), 249-251.
(36) Li, X.; Kang, L.; Li, C.; Lin, Z.; Yao, J.; Wu, Y. $PbGa_4S_7$: a wide-gap nonlinear optical material. *J. Mater. Chem. C* **2015,** 3 (13), 3060-3067.
(37) Dang, Y.; Zhong, C.; Zhang, G.; Ju, D.; Wang, L.; Xia, S.; Xia, H.; Tao, X. Crystallographic-Investigations into Properties of Acentric Hybrid Perovskite Single Crystals $NH(CH_3)_3SnX_3$ (X = Cl, Br). *Chem. Mater.* **2016,** 28 (19), 6968-6974.
(38) Gong, P.; Luo, S.; Huang, Q.; Yang, Y.; Jiang, X.; Liang, F.; Chen, C.; Lin, Z. An alkaline tin(II) halide compound $Na_3Sn_2F_6Cl$: Synthesis, structure, and characterization. *J. Solid State Chem.* **2017,** 248, 104-108.
(39) *Crystal Clear*, Rigaku Corporation: Tokyo, 2008.
(40) Farrugia, L. J. WinGX and ORTEP for Windows: an update. *J. Appl. Crystallogr.* **2012,** 45, 849-854.
(41) Sheldrick, G. M. A short history of SHELX. *Acta Crystallographica Section A* **2008,** 64, 112-122.
(42) Spek, A. L. Single-crystal structure validation with the program PLATON. *J. Appl. Crystallogr.* **2003,** 36, 7-13.
(43) Kurtz, S. K.; Perry, T. T. A powder technigue for evaluation of nonlinear optical materials. *J. Appl. Phys.* **1968,** 39 (8), 3798.
(44) Clark, S. J.; Segall, M. D.; Pickard, C. J.; Hasnip, P. J.; Probert, M. J.; Refson, K.; Payne, M. C. First principles methods using CASTEP. *Z. Kristallogr.* **2005,** 220 (5-6), 567-570.
(45) Perdew, J. P.; Burke, K.; Wang, Y. Generalized gradient approximation for the exchange-correlation hole of a many-electron system. *Phys. Rev. B* **1996,** 54 (23), 16533-16539.
(46) Hammer, B.; Hansen, L. B.; Norskov, J. K. Improved adsorption energetics within density-functional theory using revised Perdew-Burke-Ernzerhof functionals. *Phys. Rev. B* **1999,** 59 (11), 7413-7421.
(47) Lin, J. S.; Qteish, A.; Payne, M. C.; Heine, V. Optimized and Transferable Nonlocal Separable Abinitio Pseudopotentials. *Phys. Rev. B* **1993,** 47 (8), 4174-4180.
(48) Monkhorst, H. J.; Pack, J. D. Special Points for Brillouin-Zone Integrations. *Phys. Rev. B* **1976,** 13 (12), 5188-5192.
(49) *Inorganic Crystal Structure Database*, 2017-1; 2017.
(50) Li, G.; Wu, K.; Liu, Q.; Yang, Z.; Pan, S. $Na_2ZnGe_2S_6$: A New Infrared Nonlinear Optical Material with Good Balance between Large Second-Harmonic Generation Response and High Laser Damage Threshold. *J. Am. Chem. Soc.* **2016,** 138 (23), 7422-7428.
(51) Lin, X.; Zhang, G.; Ye, N. Growth and Characterization of $BaGa_4S_7$: A New Crystal for Mid-IR Nonlinear Optics. *Cryst. Growth Des.* **2009,** 9 (2), 1186-1189.
(52) Yao, J.; Mei, D.; Bai, L.; Lin, Z.; Yin, W.; Fu, P.; Wu, Y. $BaGa_4Se_7$: A New Congruent-Melting IR Nonlinear Optical Material. *Inorg. Chem.* **2010,** 49 (20), 9212-9216.
(54) Wang, C. S.; Klein, B. M. 1st-principles electronic- structure of Si, Ge, GaP, GaAs, ZnS, and ZnSe .2. optical-properties. *Phys. Rev. B* **1981,** 24 (6), 3417-3429.
(54) Chen, C. T. S., T.; Li, R. K.; Wu, Y. C.; Lin, Z. S.; Mori, Y.; Hu, Z. G.; Wang, J. Y.; Uda, S.; Yoshimura, M.; Kaneda, Y. *Nonlinear Optical Borate Crystals*. Wiley-VCH press: Germany, 2012.

For Table of Contents Only

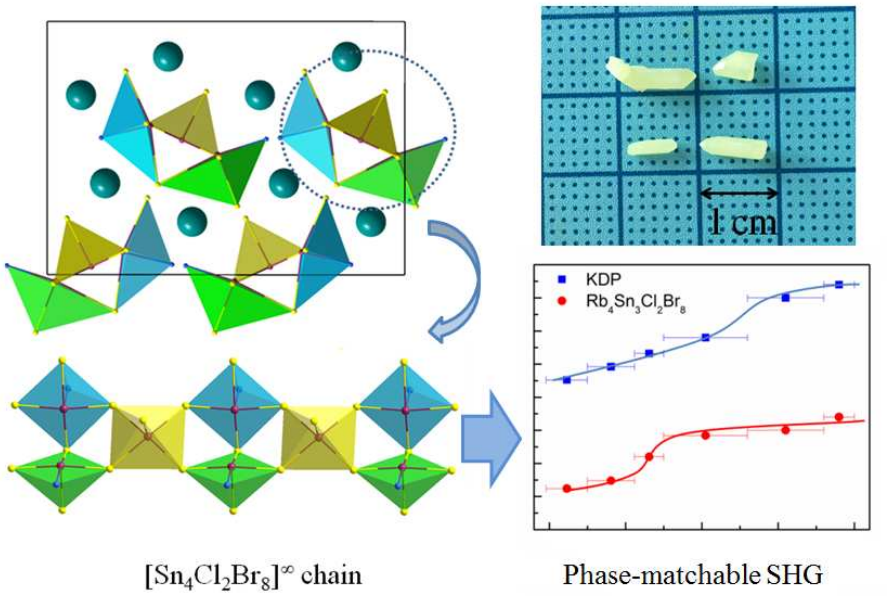

The first phase-matchable Sn-based metal halides NLO material, $Rb_4Sn_3Cl_2Br_8$, is synthesized. Its fundamental building units $[SnBr_5]$ and $[SnClBr_4]$ hold the pyramidal configuration and are found for the first time. Moreover, the 1D structure in $Rb_4Sn_3Cl_2Br_8$ has led to the phase-matchable SHG, which is beneficial to further phase-matchable nonlinear optical materials exploration in this field.